ACS OMEGA

http://pubs.acs.org/journal/acsodf

Article

Experimental Design and Response Surface Methodology Applied to Graphene Oxide Reduction for Adsorption of Triazine Herbicides

Martina Foschi, Paola Capasso, Maria Anna Maggi, Fabrizio Ruggieri, and Giulia Fioravanti*

Cite This: https://doi.org/10.1021/acsomega.1c01877

Read Online

ACCESS | Metrics & More | Article Recommendations

ABSTRACT: In this work, pristine graphene oxide and its thermally reduced derivatives, rGO, were tested for the removal of triazines (atraton, prometryn, and atrazine) from water. The reduction process was optimized by means of design of experiments (DOE) coupled with response surface methodology (RSM), relying on the adsorption efficiency of the material. The optimal reduction conditions were calculated at a temperature of 110 °C maintained for 24 h; the mildest and simplest reduction protocol was chosen, as it allows in-air heat treatment with a common laboratory oven. The rGO samples were characterized before use, confirming a partial reduction process that, leaving intact most of the oxygenated functionalities on the graphene skeleton, may still allow favorable adsorption of pollutants through both hydrogen bonds and $\pi-\pi$ interactions, which result from a large conjugated polyaromatic system. Triazine analyses were performed by high-performance liquid chromatography (HPLC); the data obtained from the adsorption isotherms were fitted with the Langmuir and Freundlich models, highlighting a slightly different adsorption behavior of atraton and prometryn compared with atrazine. Model outcomes were also used to support the hypotheses about the adsorption process.

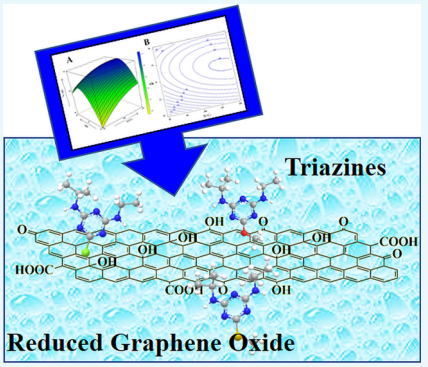

1. INTRODUCTION

The adsorption of organic pollutants is one of the promising methodologies for their removal from the environment, and in this regard, the interest toward efficient and low-cost materials for remediation of contaminants from water is strongly emerging.[1−3] Chemical oxidation, ion exchange, membrane separation and adsorption have been widely applied for the removal of pollutants from water.[4,5] Among these, adsorption remains one of the most effective and important technologies because, considering the very different nature of the treated contaminants, it has proven to be a versatile and economical method.[6−8]

Many studies have shown that graphene-based materials have good potential in the environmental field,[9] due to their unique characteristics that include the high adsorption capacity. In this respect, their large surface area and delocalized π network have been exploited in the adsorption of different types of contaminants from water.[10,11]

Pristine materials usually have a lower capability for the removal of organic pollutants compared to hybrid or polymeric composites. The explanation for this lies in the improved physicochemical properties of composite materials, which exhibit amplified interactions with analytes, such as hydrogen bonding and electron-donor−acceptor interactions. Furthermore, the integration with other nanomaterials (i.e., metals, oxides, polymers) allows better recovery of the adsorbent, as well as favor the degradation processes of the pollutants through different mechanisms. Many groups used magnetic graphene oxide-based nanocomposites for the removal of pollutants for sustainable water purification,[12,13] such as magnetic nanoparticles embedded into pristine GO sheets[14] or biochar-supported reduced graphene oxide composites.[15]

Recently, de Souza Antônio et al. described the adsorption process involving atrazine, as a target substrate, and graphene oxide (GO) as the sorbent material.[16] The study evaluated the changes in the adsorption capacity considering the variation of pH, concentration, temperature, and dissolved salts following the so-called "one variable at a time" (OVAT) approach, whereas, no mention is made about the recoverability of the material.

In this work, we studied the adsorption capacity of pristine materials, such as graphene oxide and reduced graphene oxide (rGO), toward organic pollutants. For this purpose, atrazine, atraton, and prometryn (shown in Figure 1a−c) were chosen, among the class of triazines, as a model of contaminants in water. Graphene-type adsorbents were used both in the form of a sponge (for GO), obtained by means of a freeze-drying process from an aqueous solution, and in the form of a thick

Received: April 8, 2021
Accepted: June 1, 2021

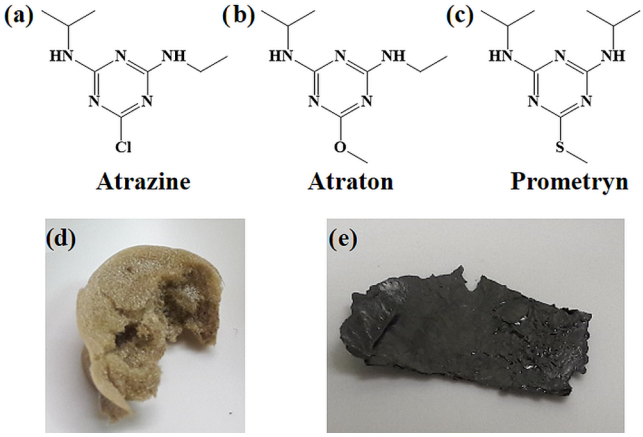

Figure 1. Triazines used in this work: (a) atrazine, (b) atraton, and (c) prometryn; graphenic materials used as sorbents: (d) pristine GO sponge obtained by freeze-drying and (e) rGO film.

film (for rGO), obtained by simple evaporation of the solvent in a Petri dish. Images of the GO sponge and the thick film of rGO are shown in Figure 1d,e (photograph taken by one of the author, G. Fioravanti, free domain).

Design of experiment (DOE) coupled with response surface methodology (RSM) has been widely used in multi-parametric optimization of different analytical methods,[17−20] including pollutant removal ones; in the latter case, attention has been paid to the optimization of adsorption working conditions (temperature, pH, time) or to the improvement of the synthesized materials.[21,22]

In this work, the DOE coupled with the RSM was chosen to optimize the graphene oxide reduction conditions to develop a useful method for the removal of triazine pesticides from the aqueous medium.

In detail, the DOE was employed to optimize the reduction process with a minimum number of experiments, attempting to obtain a material as suitable as possible for the adsorption of triazines. This methodology was chosen with the aim of optimizing a less than ideal pristine material, considering the constraints imposed by the purpose of the study on both the recoverability and reduction in air.

The rGO material was synthesized via mild heat treatment of the pristine GO, starting from acetone solution of the graphene oxide previously produced in the laboratory. The reduction conditions were optimized considering the adsorption ability of the material and by employing a three-level full factorial design to plan the representative experiments. The heat treatments were programmatically varied according to the DOE, considering a range of temperature from 80 to 120 °C and a range of dwell time from 18 to 30 h, to obtain rGO films with different thicknesses (easily recoverable material). Atrazine was chosen as the organic micropollutant model for the standardized batch adsorption tests; eventually, the optimized sorbent material was tested on other triazines, namely atraton and prometryn.

The goal of this approach would be to use a simple, easily recoverable, and environmentally friendly sorbent material obtained under the blandest possible reduction conditions, as they are easily controllable and do not require an inert atmosphere. To the best of our knowledge, there are no studies that involve pristine rGO films, thermally reduced under very mild conditions, for atrazine adsorption.

The results of the DOE model were exploited to better understand the effects that the reduction parameters have on the adsorption properties of the material. Eventually, the adsorption of the triazines was analyzed using both the Langmuir and Freundlich models. The percentage of analyte adsorption did not reach impressive values, probably due to the use of a not-quite idoneous pristine material in the form of a film (which has a lower adsorption ability than sponge). Nevertheless, the study could encourage the use of multivariate methodologies for the synthesis of different sorbent materials and can surely be a starting point for further works regarding the optimization of the adsorption process.

2. MATERIALS AND METHODS

GO was prepared from graphite flakes, with an average particle size of 100 meshes, purchased from Sigma Aldrich (graphite, quality level 100, product no. 332461). Concentrated sulfuric acid (H_2SO_4, 96%, product no. 30743), sodium nitrate ($NaNO_3$, 99%, product no. 221341), potassium permanganate ($KMnO_4$, >99%, product no. 60458), hydrogen peroxide solution (H_2O_2, 30%, product no. 95294), and hydrochloric acid (HCl, 37%, product no. 30721), atrazine (product no. 45330, PESTANAL), atraton (product no. 31206, PESTANAL), prometryn (product no. 45636, PESTANAL) and acetonitrile (product no. 34888, HPLC-grade Chromasolv) were purchased from Sigma Aldrich (St Louis, MO). All of the aqueous solutions were prepared using ultrapure MilliQ distilled water (Millipore, Bedford, MA).

2.1. GO/rGO Preparation and Characterization.

Graphene oxide was synthesized using a modified Hummers method.[23,24] Graphite (5 g) and sodium nitrate (3.8 g) were placed in a beaker in a salt/ice bath. Subsequently, 375 mL of concentrated sulfuric acid was added. The reaction mixture was kept under continuous agitation using a mechanical stirrer. After the mixture became homogeneous, 25 g of potassium permanganate was slowly added. The solution was kept stirring for 5 days at room temperature. After 5 days a 5% H_2SO_4 aqueous solution (700 mL) was poured through a funnel and H_2O_2 (30 wt %) was added drop by drop to remove potassium permanganate and the suspension was thus stirred for another 2 h. To obtain a clean product, the mixture was diluted with 5% H_2SO_4 (2 L) and left to settle for 1 day. Inorganic impurities were removed through successive centrifugation, after removing the supernatant. The solid part was washed/centrifuged at 4000 rpm for 10 min with a 5% aqueous solution of H_2SO_4 and H_2O_2 at 0.3% (12 times), then 4% HCl (3 times), deionized water (8 times), and finally with MilliQ water (2 times), removing the supernatant after each passage. The pH of the dispersion was monitored until it reached 6−7. Finally, the GO was transferred to acetone and dried at 50 °C for 24 h, affording 4.8 g of powder.

Reduced graphene oxide samples (rGO) were prepared by thermal treatment of GO in a laboratory oven. Acetone solutions of GO were heat-treated in air for 18−30 h at 80−120 °C (see Results and Discussion for details) to obtain thick films of rGO.

Surface topography was studied by scanning electron microscopy (SEM, Leo 1530 Gemini). The images were acquired with an acceleration voltage of the electron beam, E.H.T. = 10 kV, at different magnifications. The GO sample for the SEM was prepared by spin coating a very dilute aqueous solution (0.2 mg/mL, volume of 50 μL) of the material on a silicon substrate. The rGO film was deposited by

https://doi.org/10.1021/acsomega.1c01877
ACS Omega XXXX, XXX, XXX−XXX

drop-casting a dispersion of the material in water on the Si substrate.

X-ray diffraction (XRD) analysis was performed on a Panalytical X'Pert Pro X-ray diffractometer on dry and pulverized materials.

The Fourier transform infrared (FTIR) spectra of GO/rGO were recorded on a FTIR spectrometer (Perkin Elmer spectrophotometer Spectrum Two) equipped with a reflectance module (ATR). The samples were analyzed directly in the form of films.

The X-ray photoelectron spectroscopy (XPS) spectra were collected under ultra-high vacuum (UHV) conditions with a PHI 1257 spectrometer, equipped with a monochromatic Al Kα source ($h\nu$ = 1486.6 eV) with a pass energy of 11.75 eV, corresponding to an experimental resolution of 0.25 eV. The acquired XPS spectra have been fitted with Voigt line shapes and Shirley backgrounds. The GO/rGO samples for the XPS were prepared by drop-casting a dilute aqueous solution (1.0 mg/mL, volume of 50 μL) of the material on a gold substrate.

Brunauer−Emmett−Teller (BET) isotherm adsorption measurements were performed by a nitrogen porosimeter (Quantachrome Instrument, 2008). The device is controlled using NOVA Series Windows-Based Operating and Data Analysis Software. The measurements were performed on dry and pulverized materials.

2.2. Chromatographic Analysis. The analysis of the triazines was carried out using a high-performance liquid chromatography (HPLC) apparatus consisting of a controller pump (Waters 600) equipped with an online degasser Agilent Technologies 1220 series (Agilent Technologies, Waldbronn, Germany), an autosampler (Water 717 plus), a Security Guard Ultra Cartridge UHPLC C18 precolumn (4.6 mm id) from Phenomenex (Torrance, CA), a Kinetex XB-C18 (Phenomenex) column (250 mm length, 4.6 mm id, 5 μm particle size), and a 996-photodiode array detector (Waters). The working wavelength for quantitative analysis of each analyte was 220 nm. The elution was performed at room temperature, under a constant flow rate (1 mL/min) and isocratic conditions using a mixture (35:65, v/v) of water and acetonitrile. The chromatographic apparatus was controlled using Empower software (Waters). The analyzed solutions were filtered using HPLC filters (Whatman Spartan13/02 RC).

2.3. Adsorption Experiments. The effect of contact time on the adsorption was monitored. Preliminary kinetic tests were carried out and equilibrium was assumed when no further change in pesticide uptake was observed. Kinetics experiments on the adsorption on rGO were performed with 10 mL of aqueous solutions of pesticides at a concentration of 10 μg/mL and an adsorbent quantity of 10 mg. At time intervals of 20 min, 1 mL aliquots were taken out and filtered with 0.2 μm PTFE filters (PHENEX, Phenomenex) for HPLC analysis. The adsorption capacity reached its maximum in the first 1 h and then reached equilibrium. The batch triazine adsorption experiments were carried out at room temperature under shaking conditions. Ten milligrams of the rGO film were placed in contact with 10 mL of ultrapure water, in screw-cap glass vials, containing a single triazine. Sorption isotherm experiments were conducted with seven initial concentrations of pesticide (0.5, 1.0, 2.0, 5.0, 10, 20, and 50 μg/mL). The experiment at a concentration of 10 μg/mL was repeated in triplicate. The vials of the nine samples containing different concentrations of pesticide were simultaneously placed on an orbital shaker at 300 rpm in the dark for 1 h. After reaching equilibrium, 1 mL of solution was collected, filtered, and placed in HPLC vials to determine the equilibrium concentration (C_e, mg/L).

The adsorptions data can be understood using several approaches. The models usually applied are the Freundlich and Langmuir isotherms.[25,26] The Freundlich isotherm [eq 1] is generally used to model the removal of hydrophobic organic pollutants from water. It is an empirical equation used to define the uptake of an adsorbate occurring on a heterogeneous surface by multilayer adsorption

$$q_e = K_F C_e^{1/n} \tag{1}$$

where q_e (mg/g) is the adsorbed amount per unit mass of the adsorbent, C_e (mg/L) is the adsorbate equilibrium concentration in the solvent, K_F (Freundlich constant) indicates the multilayer adsorption capacity of adsorbent, and $1/n$ measures the adsorption intensity or surface heterogeneity of the adsorbent. It becomes more heterogeneous as gets closer to zero and homogeneous if this value approach one.[27−29] The amount of analytes adsorbed onto the adsorbent [eq 2] was established by the mass balance of the process under equilibrium conditions

$$q_e = V\frac{(C_0 - C_e)}{m} \tag{2}$$

where C_0 (mg/L) is the initial concentration, m is the mass (g) of the adsorbent, and V is the solution volume (L). The Langmuir model [eq 3] assumes uniform energy sites on the adsorbent surface and is defined by the following relationship

$$q_e = q_{max}\frac{K_L\, C_e}{1 + K_L C_e} \tag{3}$$

where q_{max} (mg/g) is the limiting amount of adsorbate per unit of adsorbent required for a monolayer coverage of the adsorbent surface and K_L, the Langmuir adsorption constant, is a binding constant related to the free energy of sorption. The reciprocal value of K_L corresponds to the concentration in the liquid phase at which half of the maximum adsorption capacity of the adsorbent is reached. The isotherm adsorption data can be described in the following linear forms of Freundlich [eq 4] and Langmuir [eq 5] models, respectively

$$\log q_e = \log K_F + \frac{1}{n}\log C_e \tag{4}$$

$$\frac{C_e}{q_e} = \frac{1}{q_{max}K_L} + \frac{C_e}{q_{max}} \tag{5}$$

thus, the model parameters in both cases can be easily obtained by the least-squares linear regression of the experimental data.

2.4. Response Surface Methodology. Response surface methodology (RSM) is a chemometric tool commonly used to graphically identify an optimum, that is the point (maximum or minimum in the experimental domain) at which the combination of the experimental variables results in the best response.[30] For optimization purpose, it is crucial to plan the experiments according to an appropriate experimental design to well describe the curvature of the quadratic model. A three-level full factorial design is frequently coupled with RSM since it ensures acceptable reliability in estimating individual and combined effects of the independent variables on the response.[31] Thus, the relationship between the response and

https://doi.org/10.1021/acsomega.1c01877
ACS Omega XXXX, XXX, XXX−XXX

these factors can be well approximated, in the limited domain, by a second-order polynomial function [eq 6]

$$Y = a_0 + a_1X_1 + a_2X_2 + a_3X_1X_2 + a_4X_1^2 + a_5X_2^2 \quad (6)$$

where Y is the response, X_i the experimental variables, and a_i the regression coefficients. Determining the model coefficients by ordinary least-squares regression, the value of the response Y can be computed at each point of the explored domain and can be plotted in a three-dimensional response surface, providing easier exploitation of the interesting information. The RSM and the three-level full factorial design were applied to assess the influence of the temperature (T) and the time (t) of the thermal treatment, performed for GO reduction, on the rGO film adsorption efficiency.

Factors and levels were defined considering previous knowledge and preliminary outcomes; the experiments were performed in random order and consisted of the nine best variable combinations and one replicate in the central point.

The material was optimized according to the adsorption efficiency of each produced rGO film obtained following the DOE. The model response (%abs) was calculated according to formula 7

$$\%\text{abs} = \frac{(C_i - C_f)}{C_i} \times 100 \quad (7)$$

where C_i and C_f (mg/L), respectively, are the initial and final concentration of atrazine in batch tests that were performed keeping the concentration of atrazine (5 mg/L), the volume (10 mL), and the amount of sorbent material (10 mg of rGO film) constant. After fitting the regression model, the response (%abs) was predicted at each point of the experimental domain and the best reduction conditions (for which a higher adsorption efficiency is associated) were graphically pinpointed by means of the response surface.

Analysis of variance (ANOVA) was performed to statistically identify the influencing factors, to evaluate the significance of the model, and the lack-of-fit. The determination coefficient (R^2), the related adjusted value (Adj-R^2), and the coefficient of determination in a leave-one-out cross-validation procedure (Q^2) were instead used to assess model adequacy and generalization. The statistical analysis was performed using R-based free software "Chemometric Agile Tool" (CAT, Chemometric Agile Tool, Leardi, R. et al 2019; http://gruppochemiometria.it/index.php/software).

3. RESULTS AND DISCUSSION

3.1. Sorbent Optimization. In this work, the adsorption of atrazine onto both the pristine GO material and on some of its thermally reduced derivatives was assessed. The pristine GO was obtained by a protocol already extensively studied in the literature[23] that led to very oxidized and hydrophilic graphene oxide (see the section on characterization), considering that the presence of a well oxidized starting material can influence the subsequent thermal reduction, which has been chosen.

In this study, we decided to work under mild thermal reduction conditions, using a simple laboratory oven, carrying out the reduction in air. The choice of such simple and replicable conditions was made to easily obtain a reduced material that does not disperse in the aqueous phase (recoverable) and without having to use more sophisticated and expensive equipment. When working under these mild conditions, it is important to have an indication of the degree of oxidation of the starting material because it has already been seen in the literature that by subjecting graphene oxide to reduction in air, up to 100−120 °C, extreme degradation of the material and loss of carbon, as amorphous or carbon dioxide, are not expected, i.e. processes that occur at higher temperatures.[32]

Before going into the details of the methodology chosen, we asked ourselves which form of the solid material was the most suitable in our case. Indeed, the synthesized GO and rGO could be used in two different 3D forms with different chemical−physical properties: the thick film and the sponge. To obtain the film, the graphenic material was placed in a crystallizer with acetone and dried. The sponge, on the other hand, was obtained after a freeze-drying process, which allows the elimination of water from an iced water solution by sublimation. The sample was frozen at a temperature of about −20 °C and brought to low pressure through a rotary pump. As the temperature of the sample increased, the ice was sublimed, obtaining a three-dimensional sponge. Both processes were simple, with the least possible deterioration of the structure and components of the substance itself.

As already mentioned, the materials have very different chemical−physical and structural characteristics. The three-dimensional sponge has a higher adsorption capacity, but with a high contact time, it is easily dispersed in an aqueous solution. The thick film shows a lower adsorption capacity than the sponge but allows easy recovery as it does not disperse in solution. In Figure 1 the two forms are shown; here, the experimental evidence of the reduction can be seen as a change in material color: from a pale brown (Figure 1d, GO sponge) to dark black (Figure 1e, rGO film).

Preliminary adsorption tests were conducted, initially, using an aqueous solution of pesticides and graphene oxide. Due to its poor hydrophobicity, the total solubilization of graphene oxide in aqueous solution had occurred, both in the form of thick film and sponge, simultaneously showing the poor adsorption capacity to atrazine. Subsequently, the material was thermally reduced (rGO) increasing its hydrophobicity and adsorption capacity, and tested in the two forms, sponge and film.

For reasons related to the recovery of the material, the thick film rGO was chosen to carry out the adsorption tests. The rGO sponge, in fact, still showed a redispersion behavior as soon as it came in contact with the aqueous phase containing the analyte, effectively preventing its separation from the medium.

To achieve the maximum adsorption capacity, the best reduction conditions were determined to obtain an optimal sorbent. An experimental multivariate design with two independent variables, time (t) and temperature (T), was used. For each independent variable, three different levels were considered. Each sample was used to evaluate the different adsorption capacities through batch tests, whereas the response surface methodology (RSM) was used to figure out the best experimental conditions.

The reduction of graphene oxide, previously synthesized, was carried out by dispersing the GO samples in acetone and placing them in a Petri dish. The samples were heat treated in air for 18−24−30 h in a laboratory oven, to obtain a well-adhered uniform film of reduced GO (rGO); the reduction temperature was chosen between 80 and 120 °C; subsequently, all of the obtained samples were used for preliminary measurements of adsorption with atrazine.

https://doi.org/10.1021/acsomega.1c01877
ACS Omega XXXX, XXX, XXX−XXX

DOE-RSM was employed to evaluate the influence of temperature and time and their combined effects on the adsorption efficiency of a thermally reduced GO film. The selected DOE consists of three levels for both temperature (80, 100, and 120 °C) and time (18, 24, and 30 h); the resulting experimental data were regressed with the reported equation [eq 8] providing the following model

$$\%abs = 44\ (\pm 2) + 4.7(\pm 1.3)T^{*} + 4.3(\pm 1.3)\ t^{*} - 2.5\ (\pm 1.6)\ Tt - 2(\pm 2)\ T^{2} - 11\ (\pm 2)\ t^{2**} \quad (8)$$

where the standard deviations of the coefficients are given in parenthesis.

All of the linear terms show relevant effects (significance level of 5%), whereas except for t^2, the other quadratic terms are not significant. A good agreement is demonstrated between the calculated %abs values and the experimental data with residues randomly distributed. The surface model exhibits a satisfactory descriptive and predictive performance as witnessed by the determination coefficient R^2 (0.963), the related adjusted value (Adj-R^2 = 0.857) and the determination coefficient in leave-one-out cross-validation (Q^2 = 0.793). Moreover, the reported results of the ANOVA (Table 1) reveal that the surface model is highly significant, according to the p-value < 0.05, and that well fits the experimental data, since the lack-of-fit p-value is greater than the significance level of 5%.

Table 1. Quadratic Model Obtained by DOE: Model Parameters with the Corresponding Significance Level Expressed by Stars (*p < 0.05, **p > 0.01), the Regression Coefficients with the Related Standard Deviation (SD), and the Determination Coefficients (R^2, Adj-R^2, Q^2); Results of the Model Analysis of Variance (ANOVA)

parameters	value ± SD	R^2	Adj-R^2	Q^2
intercept	44 ± 2			
$*X_1$	4.7 ± 1.3			
$*X_2$	4.3 ± 1.3	0.936	0.857	0.793
$X_1 \cdot X_2$	−2.5 ± 1.6			
X_1^2	−2 ± 2			
$**X_2^2$	−11± 2			
variation source	sum of squares	degrees of freedom	mean square	F-value	p-value
lack of fit	35	3	11.7	2.4	0,43
pure error	4.8	1	4.8		
model	589.4	5	117.9	11.8	0,02
residual	39.8	4	9.9		

Figure 2 displays the response surface and the related iso-response plot. It can be noted that the maximum response computed by the model does not exceed 46% of adsorption and that no improvement can be achieved by working in a temperature range between 110 and 120 °C, when the time is fixed at 24 h. Since the maximum is at the extremity of the experimental domain and that no improvement is achieved by increasing the temperature from 110 to 120 °C, it was chosen to work under the mildest possible conditions. Accordingly, the thermal reduction was conducted with the following optimal settings: T = 110 °C, t = 24 h. Furthermore, by integrating the DOE-RSM model outcomes and the information provided by the characterization of the optimal rGO film, a better understanding of the system involved in the adsorption process could be obtained. DOE-RSM allows identifying the influencing factors and evaluating the effect of the process parameters on the rGO film adsorption ability. In this respect, a direct interpretation of the effect of temperature can be made since the interaction term (Tt) and the quadratic one are statistically not significant. In detail, an improvement of the %abs can be obtained by increasing the temperature from 80 to 120 °C with an averaged effect on the response of near ten percentage points.

In general, the adsorption of organic pollutants is increased with the reduction of GO, in which the functional groups containing oxygen are more limited and there is an abundance of sp^2 structures that strengthen the $\pi-\pi$ interactions.[33]

From previous studies on samples reduced under mild conditions, it was found that at 80−120 °C the thermal reduction of a graphene oxide layer led to the loss of water of hydration and of the more labile groups present on the graphene skeleton, i.e., the epoxy groups.[34]

By heating the graphene oxide up to a maximum of 120 °C, we confirmed the epoxide ring-opening on the basal plane of the graphene oxide sheet, and the consequent loss of the hydroxyl group, as also proved by the decrease of the characteristic peak in the FTIR spectrum. The loss of further oxygenated groups can occur at much higher temperatures (above 200 °C), as already extensively described in the literature, considering the thermal behavior of the GO by means of differential thermal analysis.[35] However, given the reduction conditions chosen, it would not make sense to push the temperature to too high values in the air, since a significant amount of carbonaceous material in the form of carbon dioxide

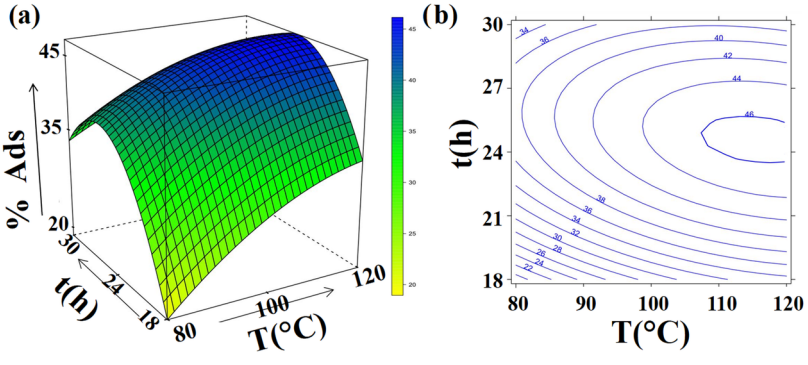

Figure 2. Surface plot (a) and related contour plot (b) of the percentage of adsorbed atrazine as a function of the reduction process parameters (temperature and time).

https://doi.org/10.1021/acsomega.1c01877
ACS Omega XXXX, XXX, XXX−XXX

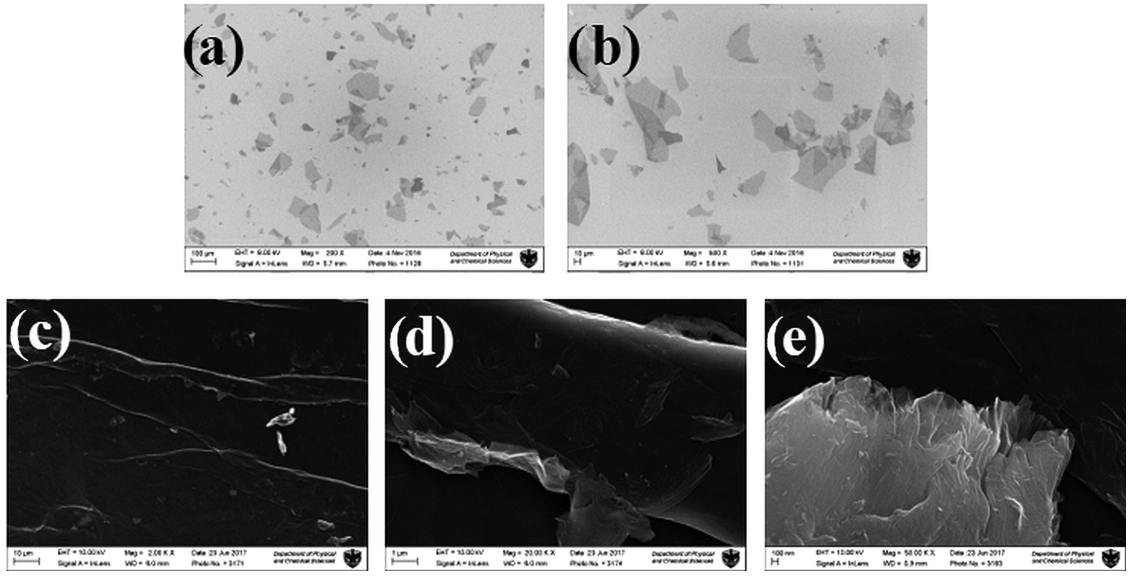

Figure 3. SEM images of GO sheets (a, b) and rGO film reduced at 110 °C (c, e).

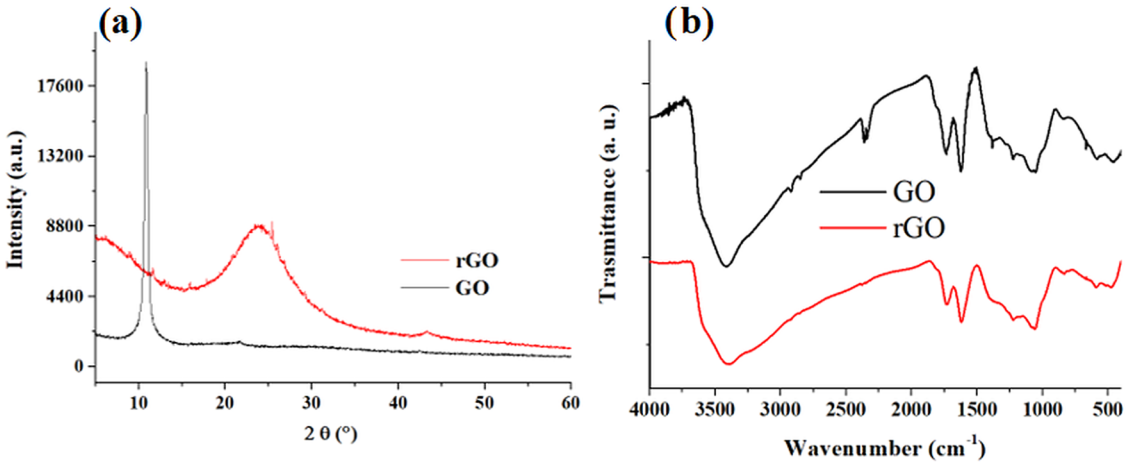

Figure 4. (a) XRD patterns of GO (black line) and rGO film reduced at 110 °C (red line) and (b) FTIR spectra of GO (black line) and rGO (red line) reduced at 110 °C.

would be lost, excessively decreasing the quality and quantity of the available adsorbent. Graphene oxide is in fact a defect-full material, with holes in its skeleton, and it is precisely in those sites that excessive deterioration of the material would occur at high temperatures in the air.

On the other hand, a quadratic trend can be confirmed with regards to the time dependence of the response, with the maximum pinpointed at t = 24 h. After 24 h it is reasonable to think that the effect of time on the reduction goes in the same direction as the temperature increase with an excessive loss of material due to oxidation in the air.

Moreover, the loss of hydrophilic oxygenated groups also reduces the possible steric hindrance between the sheets, spontaneously causing the re-aggregation of the material in the aqueous phase, and therefore decreasing the total adsorption surface of the material.

The aromatic skeleton, as well as the carboxyl, carbonyl, some residual epoxy, and hydroxy groups on rGO, remain the main sites of adsorption, which occurs reasonably through $\pi-\pi$ interactions and hydrogen bonding.

The choice of a not-so-performing material was dictated by the need to recover the adsorbent and to use a simple reduction method that can be reproduced in any research laboratory. We must also keep in mind that, as stated above, the non-optimal adsorption is also due to the re-aggregation phenomenon of the rGO sheets. Indeed, the loss of hydrophilic oxygenated groups implies, on the other hand, fewer interactions with the analyte, and therefore, lower adsorption efficiency.

3.2. Characterization of the Adsorbent Materials. Since the starting graphene oxide used is not a commercial product, we have reported the characterization of the graphene oxide from which we started. GO and rGO samples were fully characterized by scanning electron microscopy (SEM), X-ray diffraction (XRD), Fourier transform infrared (FTIR) spectroscopy, X-ray photoelectron spectroscopy (XPS), and Brunauer−Emmett−Teller (BET) surface area method. All of the reduced materials have been characterized but only the characterization relating to the reduced material at 110 °C in 24 h are reported, as from the response surface optimization.

https://doi.org/10.1021/acsomega.1c01877
ACS Omega XXXX, XXX, XXX−XXX

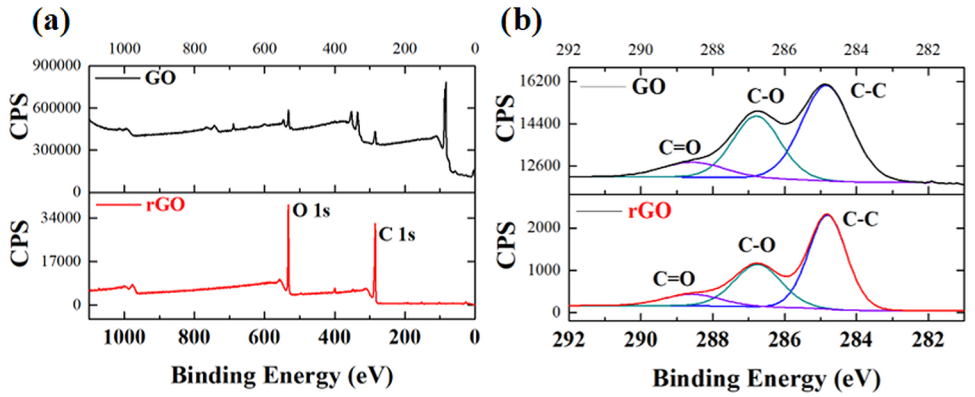

Figure 5. XPS survey of GO (upper panel, black line) and rGO (lower panel, red line) at 110 °C, (a) and C 1s region (b).

For SEM images, the starting aqueous GO solution at a concentration of 0.2 mg/mL was spin-coated on a silicon substrate, and showed a typical dispersion of graphene oxide sheets (Figure 3a,b), composed of mono and multilayers, whose lateral dimensions ranged from 100 nm to 100 μm. The GO showed the presence of some characteristic folds and ripples. The surface topography of the rGO film showed homogeneous morphology, as evidenced in Figure 3c−e, where it has been shown that the rGO film reduced at 110 °C showing some wrinkles and folds on the surface of the films.

The XRD patterns of GO shown in Figure 4a (black line) reveal a GO diffraction peak at 2θ = 11.1°, which implies an interplanar space of about 0.80 nm (calculated by Bragg equation: $d = \lambda(0.154\ \text{nm})/2\sin\theta$), corresponding to the reflection plane (001). In the rGO sample (red line), the GO signal is almost completely absent and a broader signal at 2θ = 23.9° appears, due to the decrease of intercalated oxygen functionalities after thermal reduction, corresponding to a reduced interplanar space of 0.37 nm. The graphite XRD pattern shows a single, very intense and sharp peak at 26.8°, and a characteristic interlayer spacing of 0.33 nm.

Fourier transform infrared (FTIR) analysis was performed in the wavenumber range of 4000−400 cm^{-1} for the identification of functional groups. Analyzing the rGO spectra in comparison with the starting GO we observed the presence of different absorption peaks, according to the spectra reported in the literature (Figure 4b).

The GO FT infrared spectrum (Figure 4b) evidenced the -OH stretching vibration at about 3420 cm^{-1}. The vibrational bands at 2923 and 2854 cm^{-1} are attributed to $-CH_2$. The absorption band at 1725 cm^{-1} corresponds to stretching vibrations of C═O from carbonyl or conjugated carbonyl groups. The absorption peak at 1620 cm^{-1} is assigned to the C═C (aromatics) stretching vibrations. The absorption peaks at about 1423, 1225, and 1060 cm^{-1} are assigned to −OH from carboxyl, C−O−C from epoxy or ether and C−O from alkoxy, respectively. These results are in agreement with the literature.[24]

In the 110 °C reduced GO spectrum, we saw that the absorption peaks at 1423 cm^{-1} (−OH stretching vibrations from carboxyl) in the curve of GO disappeared, and the relative intensity of C−O−C peak at 1225 cm^{-1} and C−O at 1060 cm^{-1} were lowered

FTIR analysis confirms the occurrence of the reduction process, which was not much efficient at those heating temperature conditions, leaving most of the oxygenated functionalities on the graphenic skeleton.

In Figure 5 we showed the XPS data for graphene oxide and the reduced one. From the XPS survey spectra (Figure 5a), we calculated the total content (%) of C 1s and O 1s peaks and estimated the C/O ratio that was 1.99 for GO, showing a high degree of oxidation of the material (this ratio varies according to the synthetic procedure followed and the oxidizing system chosen).

The C/O ratio calculated was 2.51 for reduced GO at 110 °C (see Table 2), a slightly higher value than the oxidized sample, as expected for reduced samples where some oxygenated groups are cleaved.

Table 2. XPS Survey: Atomic Percentages of C, O for GO, and rGO Samples[a]

	XPS survey		
	C 1s (%)	O 1s (%)	C/O ratio
GO	64.6	32.4	1.99
rGO @ 110 °C	68.7	27.4	2.51
	C 1s fitting relative area percentage (%)		
	C−C	C−O	C═O
GO	53.7	35.1	11.3
rGO @ 110 °C	57.8	30.9	11.3

[a]Analysis of the deconvoluted C 1s peaks obtained from XPS and relative area percentages for GO and rGO samples.

The XPS C 1s core level spectra are displayed in Figure 5b. The spectrum was fitted by the sum of three components assigned to C atoms belonging to: aromatic rings and hydrogenated carbon (C═C/C−C, 284.8 eV), hydroxyl and epoxy groups (C−O/C−O−C, 286.9 eV) and carbonyl groups (C═O, 288.2 eV). In Table 2 are shown, in detail, the relative percentage of deconvoluted C 1s peaks contributing to the GO and rGO samples.

In the GO sample, the relative area percentages for C−C, C−O, and C═O were, respectively, 53.7, 35.1, and 11.3 (as reported in Table 2), which confirms the presence of a high number of oxygenated groups in the starting sample. Going into detail, we can see the contributions of the hydroxyl and epoxy groups on the carbonaceous skeleton, which makes the peak relative to the C−O very intense.

From the analysis of deconvoluted peaks, we noticed in the 110 °C reduced sample an increase from 53.7% to 57.8% of the C−C contribution, while the C−O signal becomes broader and reduced in intensity, decreasing from 35.1% to 30.9%. This

https://doi.org/10.1021/acsomega.1c01877
ACS Omega XXXX, XXX, XXX−XXX

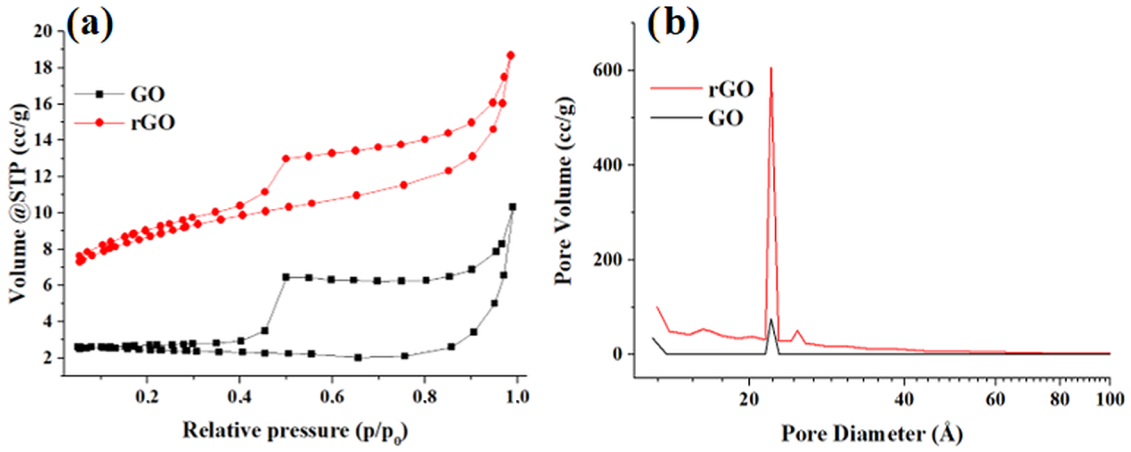

Figure 6. BET isotherm (a) for GO (black square) and rGO (red circle) and (b) BJH pore average volume and diameter of GO (black line) and rGO (red line).

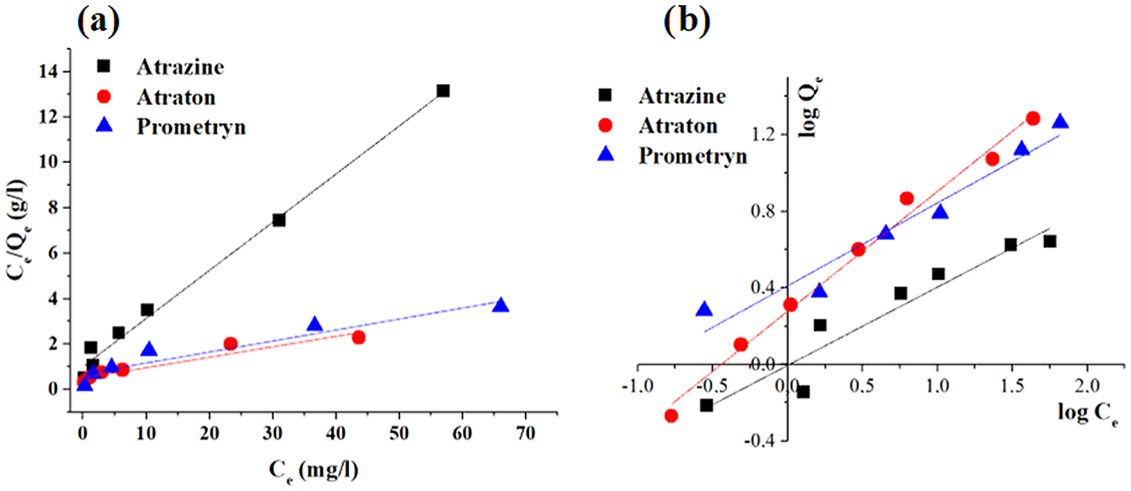

Figure 7. Adsorption isotherm plots described according to the linearized adsorption models of Langmuir (a) and Freundlich (b) and reported for all of the involved triazines.

confirms the (partly) reduction of graphene oxide to graphene-like sheets by removing the oxygen-containing groups with the recovery of a conjugated structure. The peak relative to the C═O double bond is superimposed on the peak relative to the C−O signal, and its contribution is difficult to deconvolve.

The decrease in the C−O relative abundance is preferably due to cleavage of the more labile oxygenated groups in graphene oxide, such as C−O−C bond in the epoxy groups and C(═O)−OH from carboxyl, as confirmed by the FTIR data.

Through the adsorption of nitrogen gas, it was possible to evaluate the adsorption capacity and the surface area and verify the presence and size of the pores in the rGO film. The study of the specific volume of adsorbed nitrogen allows determining the specific surface area of the materials, the specific volume and the diameter of the pores. The specific surface of a solid is the surface area per unit of mass, expressed in m^2/g, which is determined using the Brauner, Emmet and Teller equation, or more simply the BET method.

Figure 6a shows the GO and rGO adsorption and desorption isotherms, in which the presence of a moderate hysteresis phenomenon is visible (more evident for GO). The isotherm has a convex shape, classified as type III, and is representative of weak adsorbent−adsorbate interactions. A classification of pores is given by the International Union of Pure and Applied Chemistry (IUPAC), which classifies them according to their size and defines: micropores with a width below 2 nm, mesopores with a width between 2 and 50 nm, and macropores with a width greater than 50 nm.

Mesopores with an average diameter of 3 nm (30 Å) were calculated, and loops of H3 type are found in both materials (GO and rGO), mostly associated with the pore shape of solids consisting of aggregated non-rigid plate-like particles.[36]

The hysteresis loop can be explained by the fact that since it is a thick film obtained by evaporation of the solvent, therefore of not a real porous material, the channels may not be completely open, this implies a different path of the gas between the adsorption and desorption phase. The measured specific surface area of the rGO sample was approximately 30 m^2/g, while for GO it was approximately 8 m^2/g.

The specific surface area of the reduced samples is lower than that of the theoretical monolayer graphene oxide reported in the literature which ranged from 2−1000 m^2/g,[37] potentially due to the aggregation of the graphenic sheets which can cause their partial overlap and coalescence, especially the smaller ones, lowering the surface area of the material. However, the presence of a crumpled three-dimensional structure of the sheets still leaves many exposed surface areas.

https://doi.org/10.1021/acsomega.1c01877
ACS Omega XXXX, XXX, XXX−XXX

With the BJH numerical integration method (Barrett, Joyner, Halenda), the average volume and the average diameter of the pores were assessed, both in the adsorption phase and in the desorption phase (Figure 6b). From the data obtained, mesopores with an average diameter of 3 nm (30 Å) and an average volume of 0.023 cm^3/g are found both in the adsorption phase and in the desorption phase of rGO.

3.3. Adsorption Isotherm. The adsorption conditions of the triazines were standardized trying to minimize the effect due to a change in pH or ionic strength. It was chosen to work in ultrapure milliQ water at room temperature, an environment in which it is reasonable to think that most of the variables that can influence adsorption have been minimized and/or fixed. Most of the adsorption sites were saturated, but subsequent studies on real samples may serve to verify this hypothesis

The adsorption of the triazines onto the rGO film is studied using the linear form of Freundlich and Langmuir models (eqs 4 and 5). Figure 7a displays the observed adsorption equilibrium data on rGO, fitted with the Langmuir model, while Figure 7b shows the data of the three herbicides interpolated with the Freundlich model.

The adsorption parameters obtained by applying both models to each of the examined herbicides and the determination coefficients (R^2) of the linear fits are summarized in Table 3.

Table 3. Adsorption Parameters Computed Following the Linearized Langmuir (q_{max}; K_L) and Freundlich ($1/n$; K_F) Models, Their Respective Standard Errors (SE) and Determination Coefficients (R^2), which Are Reported and Computed for each of the Investigated Triazines

	Langmuir model				
pesticide	q_{max} (mg/g)	± SE	K_L (L/mg)	± SE	R^2
atrazine	4.7	0.2	0.21	0.05	0.993
atraton	22	3	0.09	0.03	0.919
prometryn	20	3	0.07	0.03	0.916
	Freundlich model				
	$1/n$	± SE	K_F (mg/g)(L/g)$^{1/n}$	± SE	R^2
atrazine	2.4	0.3	0.99	0.06	0.915
atraton	1.60	0.07	1.89	0.03	0.990
prometryn	2.3	0.3	2.57	0.06	0.951

Starting from the Langmuir model, we can assess that it fits particularly well in the case of atrazine, as evidenced by Figure 7a,b and by the high R^2 (R^2 = 0.993), demonstrating that atrazine is more in line with the assumption of the model regarding the monolayer absorption. On the other hand, the values reported in Table 3 show that the Freundlich equation fitted the adsorption data better than the Langmuir one, mainly for atraton (R^2 = 0.990) and prometryn (R^2 = 0.951). The agreement between the experimental data and those calculated according to the Freundlich model is confirmed by the R^2 values and by the small uncertainties calculated based on parameters $1/n$ and K_F (Table 3). Thus, these findings effectively demonstrate the heterogeneous enrichment of the triazines on the rGO edges and a multilayer adsorption process, at least in the case of atraton and prometryn.

The Freundlich model, consisting of points in which the heat of adsorption is reduced exponentially with the degree of coverage, is the one that best interpolates the experimental data in cases of adsorption on heterogeneous surfaces. The tendency to reach saturation can be understood as a measure of the maximum adsorbing capacity of the material that, according to the Freundlich model, is 4.4 mg/g for atrazine, 19.4 mg/g for atraton, and 18.4 mg/g for prometryn, at the maximum analyte concentration of 50 mg/l. These values are also in good agreement with the q_{max} measured in the Langmuir isotherms (respectively 4.7, 22.0, and 20.6 mg/g)

In the Freundlich models, the values of the parameter n are more than 1, this fact indicates that the adsorption process is favorable. Atraton seems to be the herbicide that shows the greatest affinity toward the rGO film. Since the triazine portion, among the investigated models, is basically the same, the greatest affinity of atraton could be explained considering the methoxy substituent of the triazine ring, which represents the strongest hydrogen bond acceptor,[38] among the studied triazines. Furthermore, the methoxy group in atraton tends to strengthen the $\pi-\pi$ interactions by enriching the electron density of the triazine ring and resulting in a more favorable multilayer adsorption process. Prometryn, despite being the most apolar, shows a significant affinity toward the material. Indeed, the presence of the thio-methyl group in prometryn could promote, also in this case, the formation of hydrogen bond in addition to $\pi-\pi$ interactions with the rGO film. Moreover, comparing the data reported in Table 3, it can be noted that the constant K_F assumes the highest value in the case of prometryn, indicating its greater tendency to exhibit multilayer adsorption. On the other hand, among the tested triazines, atrazine is the least absorbed one. The chlorine substituent in the triazine ring is, indeed, a weak hydrogen bond acceptor, and in addition, it tends to deplete the electronic density of the triazine ring due to an inductive effect, weakening the $\pi-\pi$ interactions. Accordingly, it shows the lowest affinity toward the film and a lower tendency to interact with itself. Usually, the adsorption of analogous compounds follows the trend predicted by the Lundelius rule, which establishes a general criterion, in which if a compound is less adsorbable then its solubility higher in the solvent. This can be explained by considering that the higher the solubility, the stronger the solute−solvent bond, and therefore, the lower the adsorption capacity. In our case, however, we find an inverse order of adsorption of the triazines, since atraton is more adsorbed than prometryn while atrazine is the least adsorbed. The solubility of atrazine is the lowest among the compounds studied and is equal to 33 ppm at 27 °C. The reverse behavior to that predicted by the Lundelius rule could be attributed to the ability of the substituent groups on the triazine ring to form hydrogen bonds and to influence the interactions in the multilayer adsorption process. Here, a first layer will cover the adsorbent with the analyte, saturating all possible adsorption sites; the interactions will be mainly of a secondary type, between the aromatic rings of the triazines and the conjugated polyaromatic system of the graphenic material, but the adsorbent material still contains a high number of oxygenated sites on its skeleton and can form hydrogen bonds with the analytes. Furthermore, the presence of polar groups on the surface could also contribute to the first layer adsorption through Coulomb interaction with the triazines. At this point, a subsequent layer of analyte will be able to establish favorable interactions with the adsorbed layer; these will predominantly be $\pi-\pi$ interactions between the aromatic rings of the triazines and hydrogen bonds. Going into more detail, the presence of a methoxy or thio-methyl group in atraton and prometryn can lead to favorable electrostatic interactions with the triazine ring

https://doi.org/10.1021/acsomega.1c01877
ACS Omega XXXX, XXX, XXX−XXX

amino substituents, and as stated above, can form stronger the $\pi-\pi$ interactions, favoring the adsorption process of the multilayers that follow the first one. Atrazine having a chlorine substituent on the triazine ring does not have this ability, making the $\pi-\pi$ interactions weaker, and has a low ability to exhibit a multilayer adsorption mechanism. This could explain the fact that atrazine presents a better fit to the Langmuir model and the q_{max} Langmuir trend.

Compared to the adsorption values of triazines in the literature, our values are lower, especially when considering nanocomposite materials. Examples reported in the literature include cellulose/graphene composite materials,[39] which show an adsorption efficiency of around 85% for all of the tested triazine even after several recycling procedures. Magnetic Fe_3O_4/graphene nanocomposites[13] (adsorption efficiency of 75%) and graphene oxide combined with Fe_2O_3 nanoparticles[14] (adsorption efficiency of 71%) have also been employed for triazine removal from water. With respect to these cases, the material we produced has the advantage of being easily obtained under mild conditions and without specific equipment. However, better results have been found even for a GO pristine material that, as reported by de Souza at al.,[16] reached a maximum adsorption capacity of 18.2 mg of atrazine for each gram of GO. However, it is important to emphasize that adsorption conditions as well as the physical characteristics of the material influence the recoverability of the adsorbent material (not easy recoverable in the case of GO produced by de Souza et al.) and the adsorption yield. Here, the intention to work with an easily recoverable material may have influenced the best performances of adsorption (reference is made to the choice between film and sponge). Moreover, a considerable improvement can certainly be achieved by optimizing the adsorption process through DOE and programmatically varying the influencing factors such as pH, temperature, and ionic strength.

Nevertheless, this work still is a promising starting point that can help encourage the use of multivariate strategy to produce an optimal sorbent even for pollutants having different chemical characteristics with respect to the triazine family.

4. CONCLUSIONS

Graphene and its derivatives have shown excellent performance for environmental applications due to their adsorption capacity. The key surface properties which influence the adsorption onto graphene derivatives are the surface area, $\pi-\pi$ interactions, and hydrogen bonding. The reduced graphene oxide adsorption capacity depends on the surface properties of the adsorbent itself, i.e., on the presence of sites available to interact with the pollutants (H bonding and $\pi-\pi$ interaction). The reduction process used not only leaves many oxygen-containing functional groups on the rGO but also a π-delocalized electron system, which results in a good affinity to aromatic pollutants. This was confirmed by Fourier transform infrared spectroscopy (FTIR) and X-ray photoelectron spectroscopy (XPS), where the presence of the characteristic signals of the epoxy and hydroxyl groups is confirmed, despite the slight reduction it has undergone. These groups, together with the amine pendants present on the triazine rings, may still allow favorable adsorption of these pollutants through hydrogen bonding interactions. In addition, the electrostatic interactions between the amino groups of the pesticide and the oxygen-containing functionalities of the rGO contributed to adsorption.

Dispersion of the pristine material shows an ultra-high specific surface area but no porosity, however, a revolutionary improvement in the adsorption effectiveness of graphenic materials can be achieved by introducing porosity, creating 3D structures by freeze-drying, or by forming thick films by evaporation of the solvent. Moreover, the use of thick films, rather than the simple graphene material dispersed in solution, and at the same time, the reduction of GO nanosheets allows the recovery of the adsorbent material after carrying out the adsorption tests. However, it does not represent a material with optimal characteristics for adsorption purposes because of the reduced surface area of the GO films (compared to the dispersed one) and the re-aggregation of rGO sheets in the aqueous phase. In this study, we decided to work under mild reduction conditions, using a simple laboratory oven and carrying out the reduction in air, thus working in easy and replicable conditions.

The coupling of a response surface to an experimental design, in which different parameters and different chemical−physical properties of graphenic materials can be introduced, is an original and very versatile approach to obtain an optimal sorbent. From the response surface obtained, the optimal reduction conditions of the material were reduction at a temperature of 110 °C for 24 h.

The advantage is in terms of time and experimental tests, since with the strategy just described it is possible to carry out a minimum preliminary tests to optimize the method. This also translates into economic savings, as less adsorbent material is consumed.

The Freundlich model fitted best the experimental data. The strength of adsorption of triazines followed the order: Atraton> prometryn> atrazine. Strong electron-donating abilities of O, S, and N atoms and π-bonding networks in the phenyl rings aided the adsorption.

In conclusion, this work focused on optimizing an rGO film by varying, according to DOE, the reduction working conditions. Even if the adsorption yield did not achieve sufficient levels, the study could encourage the use of multivariate methodologies for the synthesis of different sorbent materials. Indeed, graphenic material is a versatile platform, and can also provide for subsequent chemical functionalization, by means of well-known synthetic strategies

This preliminary work can be used to further optimize the graphenic materials, choosing which conditions may be the best for the adsorption of different analytes, and preparing the respective GO derivatives that best respond to the adsorption characteristics of the pollutants. By introducing functional groups that modify the surface charge of the material itself, we expected an improvement in the adsorption capacity of the sorbent material. Moreover, an extension of the work is foreseen to investigate the adsorption process by programmatically varying, again through the DOE, the adsorption conditions.

AUTHOR INFORMATION

Corresponding Author

Giulia Fioravanti − *Department of Physical and Chemical Sciences, University of L'Aquila, L'Aquila (AQ) 67100, Italy;* orcid.org/0000-0002-8653-9925; Phone: +39-0862-434244; Email: giulia.fioravanti@univaq.it

https://doi.org/10.1021/acsomega.1c01877
ACS Omega XXXX, XXX, XXX−XXX

Authors

Martina Foschi − *Department of Physical and Chemical Sciences, University of L'Aquila, L'Aquila (AQ) 67100, Italy;* orcid.org/0000-0002-7398-5221

Paola Capasso − *Department of Physical and Chemical Sciences, University of L'Aquila, L'Aquila (AQ) 67100, Italy*

Maria Anna Maggi − *Hortus Novus srl, L'Aquila (AQ) 67050, Italy;* orcid.org/0000-0003-2474-4672

Fabrizio Ruggieri − *Department of Physical and Chemical Sciences, University of L'Aquila, L'Aquila (AQ) 67100, Italy;* orcid.org/0000-0002-3677-3588

Complete contact information is available at: https://pubs.acs.org/10.1021/acsomega.1c01877

Author Contributions

G.F. and F.R. conceptualized and designed the study and drafted the initial manuscript. G.F. and P.C. contributed to the material preparation and characterization. M.F., P.C., and M.M. conducted adsorption experiments and data analysis. M.F., G.F., and F.R. contributed to the interpretation of data and critically revised the manuscript. All authors approved the final manuscript as submitted.

Funding

This research did not receive any specific grant from funding agencies in the public, commercial, or not-for-profit sectors.

Notes

The authors declare no competing financial interest.

The dataset used and/or analyzed during the current study are available from the corresponding author on reasonable request.

■ ACKNOWLEDGMENTS

The authors would like to thank all participants who contributed their time and completed laboratory study.

■ REFERENCES

(1) Xiao, F.; Pignatello, J. J. Interactions of triazine herbicides with biochar: Steric and electronic effects. *Water Res.* **2015**, *80*, 179−188.

(2) Ruggieri, F.; D'Archivio, A. A.; Di Camillo, D.; Lozzi, L.; Maggi, M. A.; Mercorio, R.; Santucci, S. Development of molecularly imprinted polymeric nanofibers by electrospinning and applications to pesticide adsorption. *J. Sep. Sci.* **2015**, *38*, 1402−1410.

(3) D'Archivio, A. A.; Maggi, M. A.; Odoardi, A.; Santucci, S.; Passacantando, M. Adsorption of triazine herbicides from aqueous solution by functionalized multiwall carbon nanotubes grown on silicon substrate. *Nanotechnology* **2018**, *29*, No. 065701.

(4) Carolin, C. F.; Kumar, P. S.; Saravanan, A.; Joshiba, G. J.; Naushad, M. Efficient techniques for the removal of toxic heavy metals from aquatic environment: A review. *J. Environ. Chem. Eng.* **2017**, *5*, 2782−2799.

(5) Jeevanantham, S.; Saravanan, A.; Hemavathy, R. V.; Kumar, P. S.; Yaashikaa, P. R.; Yuvaraj, D. Removal of toxic pollutants from water environment by phytoremediation: A survey on application and future prospects. *Environ. Technol. Innovation* **2019**, *13*, 264−276.

(6) Jung, M.; Ahn, K.; Lee, Y.; Kim, K. H.; Rhee Paeng, I.; Rhee, J.; Tae Park, J.; Paeng, K. Evaluation on the adsorption capabilities of new chemically modified polymeric adsorbents with protoporphyrin IX. *J. Chromatogr. A* **2001**, *917*, 87−93.

(7) Zhang, W. X.; Dong, M. M.; He, C. Novel electronic and planar magnetic properties of two-dimensional surface decorated antimonene. *Mater. Res. Bull.* **2019**, *118*, No. 110489.

(8) Mojiri, A.; Zhou, J. L.; Robinson, B.; Ohashi, A.; Ozaki, N.; Kindaichi, T.; Farraji, H.; Vakili, M. Pesticides in aquatic environments and their removal by adsorption methods. *Chemosphere* **2020**, *253*, No. 126646.

(9) Thakur, K.; Kandasubramanian, B. Graphene and Graphene Oxide-Based Composites for Removal of Organic Pollutants: A Review. *J. Chem. Eng. Data* **2019**, *64*, 833−867.

(10) Lu, F.; Astruc, D. Nanocatalysts and other nanomaterials for water remediation from organic pollutants. *Coord. Chem. Rev.* **2020**, *408*, No. 213180.

(11) Singh, V.; Joung, D.; Zhai, L.; Das, S. K.; Khondaker, S. I.; Seal, S. Graphene based materials: Past, present and future. *Prog. Mater. Sci.* **2011**, *56*, 1178−1271.

(12) Zhao, G. Y.; Song, S. J.; Wang, C.; Wu, Q. H.; Wang, Z. Determination of triazine herbicides in environmental water samples by high-performance liquid chromatography using graphene-coated magnetic nanoparticles as adsorbent. *Anal. Chim. Acta* **2011**, *708*, 155−159.

(13) Boruah, P. K.; Sharma, B.; Hussain, N.; Das, M. R. Magnetically recoverable Fe3O4/graphene nanocomposite towards efficient removal of triazine pesticides from aqueous solution: Investigation of the adsorption phenomenon and specific ion effect. *Chemosphere* **2017**, *168*, 1058−1067.

(14) Andrade, M. B.; Santos, T. R. T.; Silva, M. F.; Vieira, M. F.; Bergamasco, R.; Hamoudi, S. Graphene oxide impregnated with iron oxide nanoparticles for the removal of atrazine from the aqueous medium. *Sep. Sci. Technol.* **2019**, *54*, 2653−2670.

(15) Zhang, Y.; Cao, B.; Zhao, L. L.; Sun, L. L.; Gao, Y.; Li, J. J.; Yang, F. Biochar-supported reduced graphene oxide composite for adsorption and coadsorption of atrazine and lead ions. *Appl. Surf. Sci.* **2018**, *427*, 147−155.

(16) de Souza Antônio, R.; Guerra, A. C. S.; de Andrade, M. B.; Nishi, L.; Baptista, A. T. A.; Bergamasco, R.; Vieira, A. M. S. Application of graphene nanosheet oxide for atrazine adsorption in aqueous solution: synthesis, material characterization, and comprehension of the adsorption mechanism. *Environ. Sci. Pollut. Res. Int.* **2020**, 5731−5741.

(17) Tarley, C. R. T.; Silveira, G.; dos Santos, W. N. L.; Matos, G. D.; da Silva, E. G. P.; Bezerra, M. A.; Miró, M.; Ferreira, S. L. C. Chemometric tools in electroanalytical chemistry: Methods for optimization based on factorial design and response surface methodology. *Microchem. J.* **2009**, *92*, 58−67.

(18) Vera Candioti, L.; De Zan, M. M.; Cámara, M. S.; Goicoechea, H. C. Experimental design and multiple response optimization. Using the desirability function in analytical methods development. *Talanta* **2014**, *124*, 123−138.

(19) Ruggieri, F.; D'Archivio, A. A.; Foschi, M.; Maggi, M. A. Experimental Design in Ion Chromatography: Effect of the Organic Modifier and Complexing Agent on the Retention of Alkaline and Alkaline Earth Ions. *Chromatographia* **2017**, *80*, 853−860.

(20) Ruggieri, F.; D'Archivio, A. A.; Foschi, M.; Maggi, M. A. Multivariate optimization of an analytical method for the analysis of Abruzzo white wines by ICP OES. *Anal. Methods* **2020**, *12*, 2772−2778.

(21) Lingamdinne, L. P.; Vemula, K. R.; Chang, Y. Y.; Yang, J. K.; Karri, R. R.; Koduru, J. R. Process optimization and modeling of lead removal using iron oxide nanocomposites generated from bio-waste mass. *Chemosphere* **2020**, *243*, No. 125257.

(22) Bonetto, L. R.; Crespo, J. S.; Guégan, R.; Esteves, V. I.; Giovanela, M. Removal of methylene blue from aqueous solutions using a solid residue of the apple juice industry: Full factorial design, equilibrium, thermodynamics and kinetics aspects. *J. Mol. Struct.* **2021**, *1224*, No. 129296.

(23) Treossi, E.; Melucci, M.; Liscio, A.; Gazzano, M.; Samori, P.; Palermo, V. High-Contrast Visualization of Graphene Oxide on Dye-Sensitized Glass, Quartz, and Silicon by Fluorescence Quenching. *J. Am. Chem. Soc.* **2009**, *131*, 15576.

(24) Iacoboni, I.; Perrozzi, F.; Macera, L.; Taglieri, G.; Ottaviano, L.; Fioravanti, G. In situ syntheses of hydroxyapatite-grafted graphene oxide composites. *J. Biomed. Mater. Res., Part A* **2019**, *107*, 2026−2039.

(25) Freundlich, H. M. F. Over the adsorption in solution. *J. Phys. Chem. A* **1906**, *57*, 1100−1107.

(26) Langmuir, I. The constitution and fundamental properties of solids and liquids. Part I. Solids. *J. Am. Chem. Soc.* **1916**, *38*, 2221−2295.
(27) D'Archivio, A. A.; Incani, A.; Mazzeo, P.; Ruggieri, F. Adsorption of s-triazines onto polybenzimidazole: a quantitative structure-property relationship investigation. *Anal. Chim. Acta* **2009**, *650*, 175−82.
(28) Berhane, T. M.; Levy, J.; Krekeler, M. P. S.; Danielson, N. D. Kinetic sorption of contaminants of emerging concern by a palygorskite-montmorillonite filter medium. *Chemosphere* **2017**, *176*, 231−242.
(29) Nodeh, H. R.; Kamboh, M. A.; Wan Ibrahim, W. A.; Jume, B. H.; Sereshti, H.; Sanagi, M. M. Equilibrium, kinetic and thermodynamic study of pesticides removal from water using novel glucamine-calix[4]arene functionalized magnetic graphene oxide. *Environ. Sci.: Processes Impacts* **2019**, *21*, 714−726.
(30) Lundstedt, T.; Seifert, E.; Abramo, L.; Thelin, B.; Nystrom, A.; Pettersen, J.; Bergman, R. Experimental design and optimization. *Chemom. Intell. Lab. Syst.* **1998**, *42*, 3−40.
(31) Vander Heyden, Y.; Nijhuis, A.; Smeyers-Verbeke, J.; Vandeginste, B. G. M.; Massart, D. L. Guidance for robustness/ruggedness tests in method validation. *J. Pharm. Biomed. Anal.* **2001**, *24*, 723−753.
(32) Perrozzi, F.; Croce, S.; Treossi, E.; Palermo, V.; Santucci, S.; Fioravanti, G.; Ottaviano, L. Reduction dependent wetting properties of graphene oxide. *Carbon* **2014**, *77*, 473−480.
(33) Pei, Z.; Li, L.; Sun, L.; Zhang, S.; Shan, X.; Yang, S.; Wen, B. Adsorption characteristics of 1,2,4-trichlorobenzene, 2,4,6-trichlorophenol, 2-naphthol and naphthalene on graphene and graphene oxide. *Carbon* **2013**, *51*, 156−163.
(34) Catanesi, M.; Panella, G.; Benedetti, E.; Fioravanti, G.; Perrozzi, F.; Ottaviano, L.; Leandro, L. D.; Ardini, M.; Giansanti, F.; d'Angelo, M.; Castelli, V.; Angelucci, F.; Ippoliti, R.; Cimini, A. YAP/TAZ mechano-transduction as the underlying mechanism of neuronal differentiation induced by reduced graphene oxide. *Nanomedicine* **2018**, *13*, 3091−3106.
(35) Bannov, A. G.; Popov, M. V.; Kurmashov, P. B. Thermal analysis of carbon nanomaterials: advantages and problems of interpretation. *J. Therm. Anal. Calorim.* **2020**, *142*, 349−370.
(36) Bardestani, R.; Patience, G. S.; Kaliaguine, S. Experimental methods in chemical engineering: specific surface area and pore size distribution measurements—BET, BJH, and DFT. *Can. J. Chem. Eng.* **2019**, *97*, 2781−2791.
(37) Zhang, S.; Wang, H.; Liu, J.; Bao, C. Measuring the specific surface area of monolayer graphene oxide in water. *Mater. Lett.* **2020**, *261*, No. 127098.
(38) Schwöbel, J.; Ebert, R.-U.; Kühne, R.; Schüürmann, G. Prediction of the Intrinsic Hydrogen Bond Acceptor Strength of Organic Compounds by Local Molecular Parameters. *J. Chem. Inf. Model.* **2009**, *49*, 956−962.
(39) Zhang, C.; Zhang, R. Z.; Ma, Y. Q.; Guan, W. B.; Wu, X. L.; Liu, X.; Li, H.; Du, Y. L.; Pan, C. P. Preparation of Cellulose/Graphene Composite and Its Applications for Triazine Pesticides Adsorption from Water. *ACS Sustainable Chem. Eng.* **2015**, *3*, 396−405.

https://doi.org/10.1021/acsomega.1c01877
ACS Omega XXXX, XXX, XXX−XXX